Inorganic Chemistry
Article

Inorg. Chem. **2011**, *50*, 565–575 **565**
DOI: 10.1021/ic101560u

Lead−Chromium Carbonyl Complexes Incorporated with Group 8 Metals: Synthesis, Reactivity, and Theoretical Calculations

Minghuey Shieh,* Yen-Yi Chu, Miao-Hsing Hsu, Wei-Ming Ke, and Chien-Nan Lin

Department of Chemistry, National Taiwan Normal University, Taipei 116, Taiwan, Republic of China

Received August 3, 2010

The trichromium−lead complex $[Pb\{Cr(CO)_5\}_3]^{2-}$ (**1**) was isolated from the reaction of $PbCl_2$ and $Cr(CO)_6$ in a KOH/MeOH solution, and the new mixed chromium−iron−lead complex $[Pb\{Cr(CO)_5\}\{Fe(CO)_4\}_2]^{2-}$ (**3**) was synthesized from the reaction of $PbCl_2$ and $Cr(CO)_6$ in a KOH/MeOH solution followed by the addition of $Fe(CO)_5$. X-ray crystallography showed that **3** consisted of a central Pb atom bound in a trigonal-planar environment to two $Fe(CO)_4$ and one $Cr(CO)_5$ fragments. When complex **1** reacted with 1.5 equiv of $Mn(CO)_5Br$, the $Cr(CO)_4$-bridged dimeric lead−chromium carbonyl complex $[Pb_2Br_2Cr_4(CO)_{18}]^{2-}$ (**4**) was produced. However, a similar reaction of **3** or the isostructural triiron−lead complex $[Pb\{Fe(CO)_4\}_3]^{2-}$ (**2**) with $Mn(CO)_5Br$ in MeCN led to the formation of the Fe_3Pb_2-based trigonal-bipyramidal complexes $[Fe_3(CO)_9\{PbCr(CO)_5\}_2]^{2-}$ (**6**) and $[Fe_3(CO)_9\{PbFe(CO)_4\}_2]^{2-}$ (**5**), respectively. On the other hand, the Ru_3Pb_2-based trigonal-bipyramidal complex $[Ru_3(CO)_9\{PbCr(CO)_5\}_2]^{2-}$ (**7**) was obtained directly from the reaction of $PbCl_2$, $Cr(CO)_6$, and $Ru_3(CO)_{12}$ in a KOH/MeOH solution. X-ray crystallography showed that **5** and **6** each had an Fe_3Pb_2 trigonal-bipyramidal core geometry, with three $Fe(CO)_3$ groups occupying the equatorial positions and two $PbFe(CO)_4$ or $PbCr(CO)_5$ units in the axial positions, while **7** displayed a Ru_3Pb_2 trigonal-bipyramidal geometry with three equatorial $Ru(CO)_3$ groups and two axial $PbCr(CO)_5$ units. The complexes **3**−**7** were characterized spectroscopically, and their nature, formation, and electrochemistry were further examined by molecular orbital calculations at the B3LYP level of density functional theory.

Introduction

Cooperative bimetallic synergism is central to some of today's most important applications in catalysts, nanoscience, material science, and magnetism.[1−5] The cooperative properties of mixed-metal clusters are of great interest. Very few, however, are understood in detail. One important direction in this area is to rationalize the synthesis of symmetric metal or mixed-metal carbonyl clusters bearing a protective shell of CO or main-group ligands, which can be expected to exhibit reversible or quasi-reversible redox reactions without structural rearrangement of their metal skeletons.[1,3a,6]

Our research group has an ongoing interest in chromium,[7] iron,[8] and ruthenium[9] carbonyl clusters and has recently explored the lead-containing chromium system.[10] Although group 14-incorporated, group 6 and/or group 8 metal carbonyl complexes have been reported, their lead-incorporated complexes remain rare, mainly because of a lack of applicable synthetic routes.[2d,f,10−14] Furthermore, the effect and nature of homo- or heteronuclear metal−metal interactions on the formation of such carbonyl complexes remain little explored.[15,16]

*To whom correspondence should be addressed. E-mail: mshieh@ntnu.edu.tw.

(1) (a) *The Chemistry of Metal Cluster Complexes*; Shriver, D. F., Kaesz, H. D., Adams, R. D., Eds.; Wiley-VCH Publishers: New York, 1990. (b) *Metal Clusters in Chemistry*; Braunstein, P., Oro, L. A., Raithby, P. R., Eds.; Wiley-VCH Publishers: Weinheim, Germany, 1999; Vols. *1*−*3*.

(2) (a) Sinfelt, J. H. *Bimetallic Catalysts. Discoveries, Concepts and Applications*; Wiley: New York, 1983. (b) Adams, R. D.; Captain, B. *Acc. Chem. Res.* **2009**, *42*, 409–418. (c) Sivaramakrishna, A.; Clayton, H. S.; Makhubela, B. C. E.; Moss, J. R. *Coord. Chem. Rev.* **2008**, *252*, 1460–1485. (d) Thomas, J. M.; Johnson, B. F. G.; Raja, R.; Sankar, G.; Midgley, P. A. *Acc. Chem. Res.* **2003**, *36*, 20–30. (e) Pignolet, L. H.; Aubart, M. A.; Craighead, K. L.; Gould, R. A. T.; Krogstad, D. A.; Wiley, J. S. *Coord. Chem. Rev.* **1995**, *143*, 219–263. (f) Thomas, J. M.; Adams, R. D.; Boswell, E. M.; Captain, B.; Grönbeck, H.; Raja, R. *Faraday Discuss.* **2008**, *138*, 301–315. (g) Thomas, J. M.; Raja, R.; Lewis, D. W. *Angew. Chem., Int. Ed.* **2005**, *44*, 6456–6482. (h) Li, C.; Cheng, S.; Tjahjono, M.; Schreyer, M.; Garland, M. *J. Am. Chem. Soc.* **2010**, *132*, 4589–4599. (i) Park, J. H.; Chang, K.-M.; Chung, Y. K. *Coord. Chem. Rev.* **2009**, *253*, 2461–2480. (j) Xiao, J.; Puddephatt, R. J. *Coord. Chem. Rev.* **1995**, *143*, 457–500. (k) Sinfelt, J. H. *Acc. Chem. Res.* **1977**, *10*, 15–20. (l) Park, J. Y.; Zhang, Y.; Grass, M.; Zhang, T.; Somorjai, G. A. *Nano Lett.* **2008**, *8*, 673–677.

(3) (a) Femoni, C.; Iapalucci, M. C.; Kaswalder, F.; Longoni, G.; Zacchini, S. *Coord. Chem. Rev.* **2006**, *250*, 1580–1604. (b) Femoni, C.; Iapalucci, M. C.; Longoni, G.; Tiozzo, C.; Zacchini, S. *Angew. Chem., Int. Ed.* **2008**, *47*, 6666–6669. (c) Mednikov, E. G.; Jewell, M. C.; Dahl, L. F. *J. Am. Chem. Soc.* **2007**, *129*, 11619–11630. (d) Kim, J.; Lee, Y.; Sun, S. *J. Am. Chem. Soc.* **2010**, *132*, 4996–4997. (e) Yan, J.-M.; Zhang, X.-B.; Akita, T.; Haruta, M.; Xu, Q. *J. Am. Chem. Soc.* **2010**, *132*, 5326–5327. (f) Lai, F.-J.; Su, W.-N.; Sarma, L. S.; Liu, D.-G.; Hsieh, C.-A.; Lee, J.-F.; Hwang, B.-J. *Chem.—Eur. J.* **2010**, *16*, 4602–4611. (g) Hamm, G.; Becker, C.; Henry, C. R. *Nanotechnology* **2006**, *17*, 1943–1947. (h) Berenbaum, A.; Ginzburg-Margau, M.; Coombs, N.; Lough, A. J.; Safa-Sefat, A.; Greedan, J. E.; Ozin, G. A.; Manners, I. *Adv. Mater.* **2003**, *15*, 51–55.

(4) (a) Ferrando, R.; Jellinek, J.; Johnston, R. L. *Chem. Rev.* **2008**, *108*, 845–910. (b) Roucoux, A.; Schulz, J.; Patin, H. *Chem. Rev.* **2002**, *102*, 3757–3778. (c) Kobayashi, H.; Yamauchi, M.; Kitagawa, H.; Kubota, Y.; Kato, K.; Takata, M. *J. Am. Chem. Soc.* **2010**, *132*, 5576–5577. (d) Scott, R. W. J.; Sivadinarayana, C.; Wilson, O. M.; Yan, Z.; Goodman, D. W.; Crooks, R. M. *J. Am. Chem. Soc.* **2005**, *127*, 1380–1381.

Published on Web 12/13/2010

The study and comparison of lead-containing homo- or heterometallic complexes are, therefore, of great interest and are challenging in view of their cooperative chemical properties and potential applications.

In the present study, facile routes were discovered to a series of lead-containing homo- or heteronuclear chromium and group 8 trigonal-planar complexes, $[Et_4N]_2[Pb\{Cr(CO)_5\}_3]$ ($[Et_4N]_2$[**1**])[11a] and $[Bu_4N]_2[Pb\{Cr(CO)_5\}\{Fe(CO)_4\}_2]$ ($[Bu_4N]_2$[**3**]), and trigonal-bipyramidal clusters, $[Et_4N]_2[Fe_3(CO)_9\{PbFe(CO)_4\}_2]$ ($[Et_4N]_2$[**5**]), $[Et_4N]_2[Fe_3(CO)_9\{PbCr(CO)_5\}_2]$ ($[Et_4N]_2$[**6**]), and $[Et_4N]_2[Ru_3(CO)_9\{PbCr(CO)_5\}_2]$ ($[Et_4N]_2$[**7**]), in which the mixed chromium−group 8 trigonal-planar complexes could readily undergo coupling reactions to give rise to their corresponding trigonal-bipyramidal complexes. Clusters **3**, **6**, and **7** represent the first examples of lead-containing mixed chromium−group 8 metal clusters. In addition, the formation, structural transformation, and electrochemistry of the resultant clusters were investigated and discussed on the basis of density functional theory (DFT) calculations.

Results and Discussion

The class of Pb−Cr−CO complexes has previously been rare because of the lack of a feasible methodology and their reactive nature.[10,11a−g] By varying of the sources of lead(II)

(5) (a) Kahn, O. *Molecular Magnetism*; VCH: Weinheim, Germany, 1993. (b) Mathonière, C.; Sutter, J.-P.; Yakhmi, J. V. Bimetallic magnets: Present and perspectives. In *Magnetism: molecules to materials*; Miller, J. S., Drillon, M., Eds.; Wiley-VCH: Weinheim, Germany, 2002; Vol. *4*. (c) Sun, H.-L.; Wang, Z.-M.; Gao, S. *Coord. Chem. Rev*. **2010**, *254*, 1081–1100. (d) Przychodzeń, P.; Korzeniak, T.; Podgajny, R.; Sieklucka, B. *Coord. Chem. Rev*. **2006**, *250*, 2234–2260. (e) Toma, L. M.; Toma, L. D.; Delgado, F. S.; Ruiz-Pérez, C.; Sletten, J.; Cano, J.; Clemente-Juan, J. M.; Lloret, F.; Julve, M. *Coord. Chem. Rev*. **2006**, *250*, 2176–2193. (f) Ohba, M.; kawa, H. *Coord. Chem. Rev*. **2000**, *198*, 313–328. (g) Clemente-Juan, J. M.; Coronado, E. *Coord. Chem. Rev*. **1999**, *193*−*195*, 361–394. (h) Femoni, C.; Iapalucci, M. C.; Longoni, G.; Wolowska, J.; Zacchini, S.; Zanello, P.; Fedi, S.; Riccò, M.; Pontiroli, D.; Mazzani, M. *J. Am. Chem. Soc*. **2010**, *132*, 2919–2927. (i) Eichhöfer, A.; Olkowska-Oetzel, J.; Fenske, D.; Fink, K.; Mereacre, V.; Powell, A. K.; Buth, G. *Inorg. Chem*. **2009**, *48*, 8977–8984. (j) Bechlars, B.; Issac, I.; Feuerhake, R.; Clérac, R.; Fuhr, O.; Fenske, D. *Eur. J. Inorg. Chem*. **2008**, 1632–1644. (k) Miyasaka, H.; Takayama, K.; Saitoh, A.; Furukawa, S.; Yamashita, M.; Clérac, R. *Chem.—Eur. J*. **2010**, *16*, 3656–3662. (l) Prinz, M.; Kuepper, K.; Taubitz, C.; Raekers, M.; Khanra, S.; Biswas, B.; Weyhermüller, T.; Uhlarz, M.; Wosnitza, J.; Schnack, J.; Postnikov, A. V.; Schröder, C.; George, S. J.; Neumann, M.; Chaudhuri, P. *Inorg. Chem*. **2010**, *49*, 2093–2102. (m) Sutter, J.-P.; Dhers, S.; Rajamani, R.; Ramasesha, S.; Costes, J.-P.; Duhayon, C.; Vendier, L. *Inorg. Chem*. **2009**, *48*, 5820–5828. (n) Freedman, D. E.; Jenkins, D. M.; Iavarone, A. T.; Long, J. R. *J. Am. Chem. Soc*. **2008**, *130*, 2884–2885. (o) Berlinguette, C. P.; Dragulescu-Andrasi, A.; Sieber, A.; Güdel, H.-U.; Achim, C.; Dunbar, K. R. *J. Am. Chem. Soc*. **2005**, *127*, 6766–6779.

(6) (a) Wadepohl, H. *Coord. Chem. Rev*. **1999**, *185*−*186*, 551–568. (b) Cador, O.; Cattey, H.; Halet, J.-F.; Meier, W.; Mugnier, Y.; Wachter, J.; Saillard, J.-Y.; Zouchoune, B.; Zabel, M. *Inorg. Chem*. **2007**, *46*, 501–509. (c) Roth, J. D.; Lewis, G. J.; Safford, L. K.; Jiang, X.; Dahl, L. F.; Weaver, M. J. *J. Am. Chem. Soc*. **1992**, *114*, 6159–6169.

(7) (a) Cherng, J.-J.; Lee, G.-H.; Peng, S.-M.; Ueng, C.-H.; Shieh, M. *Organometallics* **2000**, *19*, 213–215. (b) Cherng, J.-J.; Lai, Y.-W.; Liu, Y.-H.; Peng, S.-M.; Ueng, C.-H.; Shieh, M. *Inorg. Chem*. **2001**, *40*, 1206–1212. (c) Shieh, M.; Cherng, J.-J.; Lai, Y.-W.; Ueng, C.-H.; Peng, S.-M.; Liu, Y.-H. *Chem.—Eur. J*. **2002**, *8*, 4522–4527. (d) Shieh, M.; Ho, L.-F.; Jang, L.-F.; Ueng, C.-H.; Peng, S.-M.; Liu, Y.-H. *Chem. Commun*. **2001**, 1014–1015. (e) Shieh, M.; Ho, L.-F.; Guo, Y.-W.; Lin, S.-F.; Lin, Y.-C.; Peng, S.-M.; Liu, Y.-H. *Organometallics* **2003**, *22*, 5020–5026. (f) Shieh, M.; Lin, S.-F.; Guo, Y.-W.; Hsu, M.-H.; Lai, Y.-W. *Organometallics* **2004**, *23*, 5182–5187. (g) Hsu, M.-H.; Miu, C.-Y.; Lin, Y.-C.; Shieh, M. *J. Organomet. Chem*. **2006**, *691*, 966–974. (h) Shieh, M.; Ho, L.-F.; Chen, P.-C.; Hsu, M.-H.; Chen, H.-L.; Guo, Y.-W.; Pan, Y.-W.; Lin, Y.-C. *Organometallics* **2007**, *26*, 6184–6196.

(8) (a) Shieh, M.; Chen, P.-F.; Tsai, Y.-C.; Shieh, M.-H.; Peng, S.-M.; Lee, G.-H. *Inorg. Chem*. **1995**, *34*, 2251–2254. (b) Shieh, M.; Shieh, M.-H.; Tsai, Y.-C.; Ueng, C.-H. *Inorg. Chem*. **1995**, *34*, 5088–5090. (c) Shieh, M; Sheu, C.-m.; Ho, L.-F.; Cherng, J.-J.; Jang, L.-F.; Ueng, C.-H.; Peng, S.-M.; Lee, G.-H. *Inorg. Chem*. **1996**, *35*, 5504–5508. (d) Shieh, M.; Tsai, Y.-C.; Cherng, J.-J.; Shieh, M.-H.; Chen, H.-S.; Ueng, C.-H.; Peng, S.-M.; Lee, G.-H. *Organometallics* **1997**, *16*, 456–460. (e) Huang, K.-C.; Shieh, M.-H.; Jang, R.-J.; Peng, S.-M.; Lee, G.-H.; Shieh, M. *Organometallics* **1998**, *17*, 5202–5205. (f) Shieh, M.; Chen, H.-S.; Chi, H.-H.; Ueng, C.-H. *Inorg. Chem*. **2000**, *39*, 5561–5564. (g) Shieh, M.; Liou, Y.; Hsu, M.-H.; Chen, R.-T.; Yeh, S.-J.; Peng, S.-M.; Lee, G.-H. *Angew. Chem., Int. Ed*. **2002**, *41*, 2384–2386. (h) Shieh, M.; Chen, H.-S.; Lai, Y.-W. *Organometallics* **2004**, *23*, 4018–4025. (i) Lai, Y.-W.; Cherng, J.-J.; Sheu, W.-S.; Lee, G.-A.; Shieh, M. *Organometallics* **2006**, *25*, 184–190. (j) Shieh, M.; Ho, C.-H.; Sheu, W.-S.; Chen, B.-G.; Chu, Y.-Y.; Miu, C.-Y.; Liu, H.-L.; Shen, C.-C. *J. Am. Chem. Soc*. **2008**, *130*, 14114–14116. (k) Shieh, M.; Miu, C.-Y.; Lee, C.-J.; Chen, W.-C.; Chu, Y.-Y.; Chen, H.-L. *Inorg. Chem*. **2008**, *47*, 11018–11031. (l) Chen, B.-G.; Ho, C.-H.; Lee, C.-J.; Shieh, M. *Inorg. Chem*. **2009**, *48*, 10757–10768.

(9) (a) Shieh, M.; Hsu, M.-H.; Sheu, W.-S.; Jang, L.-F.; Lin, S.-F.; Chu, Y.-Y.; Miu, C.-Y.; Lai, Y.-W.; Liu, H.-L.; Her, J.-L. *Chem.—Eur. J*. **2007**, *13*, 6605–6616. (b) Shieh, M.; Chu, Y.-Y.; Miu, C.-Y.; Wu, P.-F.; Zeng, T.-M. *Dalton Trans*. **2010**, *39*, 1492–1503.

(10) Hsu, M.-H.; Chen, R.-T.; Sheu, W.-S.; Shieh, M. *Inorg. Chem*. **2006**, *45*, 6740–6747.

(11) (a) Rutsch, P.; Huttner, G. *Angew. Chem., Int. Ed*. **2000**, *39*, 2118–2120. (b) Rutsch, P.; Huttner, G. *Z. Naturforsch., B: Chem. Sci*. **2002**, *57b*, 25–42. (c) Kircher, P.; Huttner, G.; Schiemenz, B.; Heinze, K.; Zsolnai, L.; Walter, O.; Jacobi, A.; Driess, A. *Chem. Ber*. **1997**, *130*, 687–699. (d) Eichhorn, B. W.; Haushalter, R. C. *J. Chem. Soc., Chem. Commun*. **1990**, 937–938. (e) Seidel, N.; Jacob, K.; Fischer, A. K. *Organometallics* **2001**, *20*, 578–581. (f) Pu, L.; Power, P. P.; Boltes, I.; Herbst-Irmer, R. *Organometallics* **2000**, *19*, 352–356. (g) Kircher, P.; Huttner, G.; Heinze, K.; Schiemenz, B.; Zsolnai, L.; Büchner, M.; Driess, A. *Eur. J. Inorg. Chem*. **1998**, 703–720. (h) Kircher, P.; Huttner, G.; Heinze, K.; Renner, G. *Angew. Chem., Int. Ed*. **1998**, *37*, 1664–1666. (i) Veith, M.; Weidner, S.; Kunze, K.; Käfer, D.; Hans, J.; Huch, V. *Coord. Chem. Rev*. **1994**, *137*, 297–322. (j) Brice, M. D.; Cotton, F. A. *J. Am. Chem. Soc*. **1973**, *95*, 4529–4532. (k) Kesanli, B.; Fettinger, J.; Eichhorn, B. *Chem.—Eur. J*. **2001**, *7*, 5277–5285. (l) Hitchcock, P. B.; Lappert, M. F.; McGeary, M. J. *Organometallics* **1990**, *9*, 884–886.

(12) (a) Cassidy, J. M.; Whitmire, K. H. *Inorg. Chem*. **1989**, *28*, 2494–2496. (b) Whitmire, K. H.; Lagrone, C. B.; Churchill, M. R.; Fettinger, J. C.; Robinson, B. H. *Inorg. Chem*. **1987**, *26*, 3491–3499. (c) Lagrone, C. B.; Whitmire, K. H.; Churchill, M. R.; Fettinger, J. C. *Inorg. Chem*. **1986**, *25*, 2080–2085. (d) Herberhold, M.; Trobs, V.; Milius, W.; Wrackmeyer, B. *Z. Naturforsch., B: Chem. Sci*. **1994**, *49*, 1781–1788. (e) Reina, R.; Rossell, O.; Seco, M.; Pellinghelli, M. A.; Tiripicchio, A.; de Montauzon, D. *Organometallics* **1996**, *15*, 5347–5349. (f) Veith, M.; Hans, J. *Angew. Chem., Int. Ed. Engl*. **1991**, *30*, 878–880. (g) Lentz, D.; Brüdgam, I.; Hartl, H. *Angew. Chem., Int. Ed. Engl*. **1985**, *24*, 119–120. (h) Anema, S. G.; Mackay, K. M.; Nicholson, B. K. *J. Chem. Soc., Dalton Trans*. **1996**, 3853–3858. (i) Haupt, H.-J.; Flörke, U. *Acta Crystallogr*. **1988**, *C44*, 472–474. (j) Anema, S. G.; Mackay, K. M.; Nicholson, B. K.; Van Tiel, M. *Organometallics* **1990**, *9*, 2436–2442. (k) McNeese, T.; Wreford, S. S.; Tipton, D. L.; Bau, R. *J. Chem. Soc., Chem. Commun*. **1977**, 390–391. (l) Haupt, H.-J.; Götze, A.; Flörke, U. *Z. Anorg. Allg. Chem*. **1988**, *557*, 82–90. (m) Flörke, U.; Haupt, H.-J. *Z. Kristallogr*. **1992**, *201*, 301–303. (n) Gusbeth, P.; Vahrenkamp, H. *Chem. Ber*. **1985**, *118*, 1746–1757. (o) Gusbeth, P.; Vahrenkamp, H. *Chem. Ber*. **1985**, *118*, 1770–1781. (p) Adams, R. D.; Brice, M. D.; Cotton, F. A. *Inorg. Chem*. **1974**, *13*, 1080–1085. (q) Balch, A. L.; Olmstead, M. M.; Oram, D. P. *Inorg. Chem*. **1988**, *27*, 4309–4312.

(13) (a) Adams, R. D.; Captain, B.; Fu, W. *J. Organomet. Chem*. **2003**, *671*, 158–165. (b) Aarnts, M. P.; Stufkens, D. J.; Oskam, A.; Fraanje, J.; Goubitz, K. *Inorg. Chim. Acta* **1997**, *256*, 93–105. (c) Burton, N. C.; Cardin, C. J.; Cardin, D. J.; Twamley, B.; Zubavichus, Y. *Organometallics* **1995**, *14*, 5708–5710. (d) Adams, R. D.; Boswell, E. M.; Captain, B.; Hungria, A. B.; Midgley, P. A.; Raja, R.; Thomas, J. M. *Angew. Chem., Int. Ed*. **2007**, *46*, 8182–8185. (e) Adams, R. D.; Captain, B.; Hall, M. B.; Trufan, E.; Yang, X. *J. Am. Chem. Soc*. **2007**, *129*, 12328–12340. (f) Hermans, S.; Johnson, B. F. G. *Chem. Commun*. **2000**, 1955–1956. (g) Ball, R.; Bennett, M. J. *Inorg. Chem*. **1972**, *11*, 1806–1811. (h) Kabir, S. E.; Raha, A. K.; Hassan, M. R.; Nicholson, B. K.; Rosenberg, E.; Sharmin, A.; Salassa, L. *Dalton Trans*. **2008**, 4212–4219. (i) Cardin, C. J.; Cardin, D. J.; Convery, M. A.; Dauter, Z.; Fenske, D.; Devereux, M. M.; Power, M. B. *J. Chem. Soc., Dalton Trans*. **1996**, 1133–1144. (j) Howard, J. A. K.; Kellett, S. C.; Woodward, P. *J. Chem. Soc., Dalton Trans*. **1975**, 2332–2334.

(14) (a) Whitmire, K. H. *J. Coord. Chem*. **1988**, *17*, 95–203. (b) Compton, N. A.; Errington, R. J.; Norman, N. C. *Adv. Organomet. Chem*. **1990**, *31*, 91–182.

(15) Harrison, P. G. *Comprehensive Organometallic Chemistry II*; Abel, E. W., Stone, F. G. A., Wilkinson, G., Eds.; Pergamon Press: Oxford, U.K., 1995; Vol. *2*, Chapter 7.

(16) Pauling, L. *The Nature of the Chemical Bond*, 3rd ed.; Cornell University: Ithaca, NY, 1960; p 257.

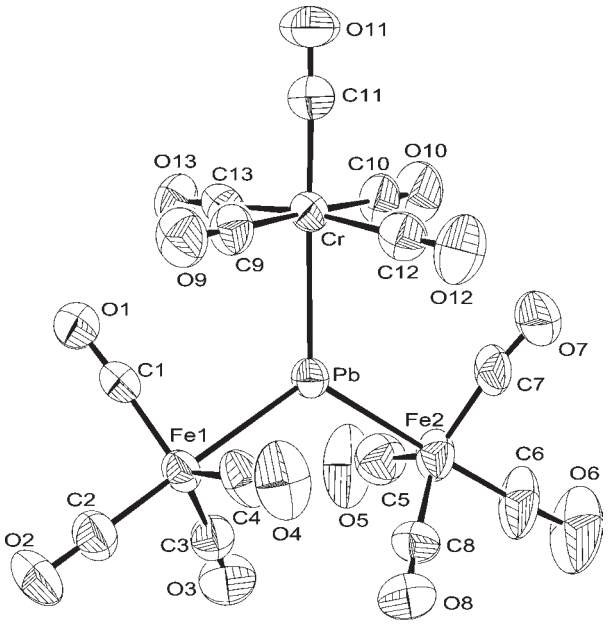

Figure 1. ORTEP diagram of anion **3**, showing 30% probability thermal ellipsoids. Selected bond lengths (Å) and angles (deg): Pb1−Cr1 2.714(2), Pb1−Fe1 2.656(2), Pb1−Fe2 2.636(2); Cr1−Pb1−Fe1 118.67(6), Cr1−Pb1−Fe2 123.67(7), Fe1−Pb1−Fe2 117.03(7).

Scheme 1

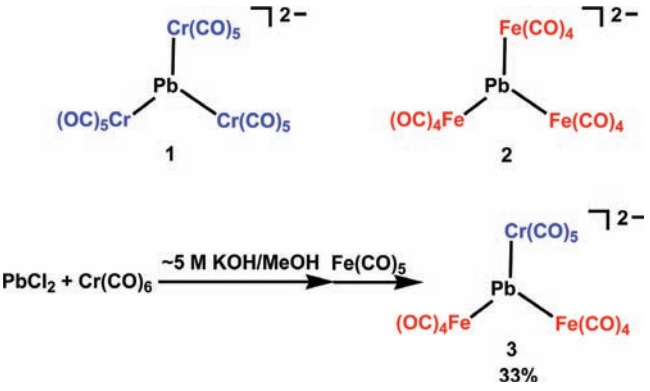

and the bases, as well as the concentration of the bases applied, we have discovered a facile route to the known lead−chromium carbonyl complex $[Pb\{Cr(CO)_5\}_3]^{2-}$ (**1**)[11a] from the reaction of $PbCl_2$ with $Cr(CO)_6$ in a KOH/MeOH solution. In pursuit of novel heteronuclear clusters, group 8 metals were introduced into the lead−chromium carbonyl system. It was found that when $PbCl_2$ was treated with $Cr(CO)_6$ in a KOH/MeOH solution, followed by the addition of $Fe(CO)_5$, the mixed chromium−iron−lead complex $[Pb\{Cr(CO)_5\}\{Fe(CO)_4\}_2]^{2-}$ (**3**) could be obtained in moderate yields (Scheme 1). Complex **3** was quite air-sensitive and was isolated as the salt $[Bu_4N]^+$. Complex **3** was characterized by spectroscopic methods, elemental analysis, and single-crystal X-ray diffraction analysis. An ORTEP diagram of the molecular structure of the anion **3** is shown in Figure 1.

The anion **3** is structurally similar to complex **1**[11a] and the previously known triiron−lead complex **2**.[12a] The average Pb−Fe bond length in **3** [2.65(1) Å] is comparable to those in **2** [2.624(4) Å] and $[Et_4N]_2[Pb\{Fe_2(CO)_8\}\{Fe(CO)_4\}_2]$ [2.7(1) Å][12c] (Table 1). The Pb−Cr bond length of **3**, 2.714(2) Å, is close to those in **1** [average 2.729(4) Å] and the metalloplumbylene complex $[(FcN)_2PbCr(CO)_5]$ [2.7157(4) Å; FcN = $[Fe(\eta^5\text{-}C_5H_5)(\eta^5\text{-}C_5H_3(CH_2NMe_2)\text{-}2)\text{-}C,N]$].[11e] Complex **3** is an isoelectronic analogue of **1** and **2**, which contain three unsaturated Pb−M (M = Cr, Fe) bonds in terms of the electron-counting rule.[11a,12a] These three isostructural complexes, **1**−**3**, thus provided good precursors for the preparation of polynuclear clusters.

Previous studies showed that the trigonal-planar $PbCr_3$−**1** complex could react with the nucleophilic reagent PMe_3 to form its base adduct $[Pb\{Cr(CO)_5\}_3(PMe_3)]^{2-}$.[11a] For comparison, and to explore possible metal expansion reactions, the reactions of the trigonal-planar compounds **1**−**3** with $Mn(CO)_5Br$ were studied. When complex **1** was treated with $Mn(CO)_5Br$ at ambient temperature, a new ring complex, $[Pb_2Br_2Cr_4(CO)_{18}]^{2-}$ (**4**), was produced with the elimination of $Mn_2(CO)_{10}$ and $[HCr_2(CO)_{10}]^-$ (identified by IR spectroscopy). The results suggested that the central Pb atom was nucleophilically attacked by Br^- accompanied with the loss of $[Cr(CO)_5]^{2-}$, followed by a coupling reaction to give complex **4**. Complex **4** could be further transformed to the known tetrahedral compound $[PbBr_2Cr_2(CO)_{10}]^{2-}$[11b] via Pb−Cr bond breakage and Pb−Br bond formation, upon the addition of $Mn(CO)_5Br$ in a MeCN solution (Scheme 2).

Compound **4** was characterized by IR spectroscopy, elemental analysis, and single-crystal X-ray diffraction. As shown in Figure 2, the anion **4** contains an inversion center at the center of the Pb_2Cr_2 plane, in which the Pb1−Cr2−Pb1a and Cr2−Pb1−Cr2a angles are 109.79(5) and 70.21(5)°, respectively. The Pb atom is four-coordinated but severely distorted from the ideal tetrahedral geometry [70.21(5)−135.81(6)°]. With respect to the bonding, complex **4** may be considered to be composed of two $[\{(CO)_5Cr\}PbBr\{Cr(CO)_4\}]^-$ species, which are dimerized by the Pb−Cr bonding to form a four-membered Pb_2Cr_2 ring due to the electron deficiency of the Pb atoms. According to a search of the Cambridge Crystallographic Data Centre, complex **4** is the first example of a four-membered Pb_2M_2 ring in the lead−group 6 metal system. The Pb−$Cr(CO)_4$ distances in **4** [average 2.72(1) Å] are slightly longer than the Pb−$Cr(CO)_5$ distances [2.679(2) Å], indicating that the Pb−$Cr(CO)_4$ bonds in the Pb_2Cr_2 ring are weaker than the pendent Pb−$Cr(CO)_5$ bonds. As a result, complex **4** was susceptible to the attack of Br^- onto the central Pb_2Cr_2 ring, causing Pb−Cr bond cleavage to give $[PbBr_2Cr_2(CO)_{10}]^{2-}$.

For comparison, an isostructural trigonal-planar complex $[Pb\{Fe(CO)_4\}_3]^{2-}$ (**2**)[12a] was synthesized. The treatment of complex **2** with $Mn(CO)_5Br$ in MeCN at 80 °C led to the formation of the trigonal-bipyramidal cluster $[Fe_3(CO)_9\{PbFe(CO)_4\}_2]^{2-}$ (**5**; Scheme 3). Complex **5** was considered as a result of the coupling reaction of **2** via Pb−Fe and Fe−Fe bond formation and the loss of one $[Fe(CO)_4]^{2-}$ and three CO units. In a similar fashion, reaction of the chromium−iron planar complex **3** with $Mn(CO)_5Br$ in MeCN at 80 °C yielded the mixed chromium−iron trigonal-bipyramidal cluster $[Fe_3(CO)_9\{PbCr(CO)_5\}_2]^{2-}$ (**6**; Scheme 3). Likewise, cluster **6** could be regarded as a result of the dimerization of **3** via Pb−Fe and Fe−Fe bond formation and the loss of one $[Fe(CO)_4]^{2-}$ and three CO units. Both clusters **5** and **6** were isolated as the salt $[Et_4N]^+$, and they were fully characterized by IR spectroscopy, elemental analyses, and single-crystal X-ray diffraction. It is of great interest that clusters **5** and **6** were interconvertible under suitable conditions. Cluster **5** readily transformed to cluster **6** in good yields upon treatment with $Cr(CO)_6$ in a

Table 1. Average Bond Distances (Å) of $[PPh_4]_2$[**1**], $[Et_4N]_2$[**2**], $[Bu_4N]_2$[**3**], $[Et_4N]_2$[**4**], $[Et_4N]_2$[**5**], $[Et_4N]_2$[**6**], $[Et_4N]_2$[**7**], and Related Complexes

complex	Fe−Fe	Ru−Ru	Pb−Cr	Pb−Fe	Pb−Ru	ref
$[PPh_4]_2$[**1**]			2.729(4)			11a
$[Et_4N]_2$[**2**]				2.624(4)		12a
$[Bu_4N]_2$[**3**]			2.714(2)	2.65(1)		*a*
$[Et_4N]_2$[**4**]			2.72(1)[b]			*a*
			2.679(2)[c]			
$[Et_4N]_2$[**5**]	2.83(4)			2.60(1)[d]		*a*
				2.546(2)[e]		
$[Et_4N]_2$[**6**]	2.79(6)		2.67(1)	2.65(3)		*a*
$[Et_4N]_2$[**7**]		2.97(1)	2.680(4)		2.77(2)	*a*
$[Et_4N]_2[Pb\{Fe_2(CO)_8\}\{Fe(CO)_4\}_2]$	2.617(5)			2.7(1)		12c
$(FcN)_2PbCr(CO)_5$[f]			2.7157(4)			11e
$[PPh_4]_2[PbBr_2Cr_2(CO)_{10}]$			2.70(2)			11b
$Fe_3(CO)_9(\mu_3\text{-}CF)_2$	2.540(2)					12g
$Fe_3(CO)_9[\mu_3\text{-}SiFeCp(CO)_2]_2$	2.67(2)					12j
$Fe_3(CO)_9(\mu_3\text{-}GeEt)_2$	2.73(1)					12j
$Fe_3(CO)_9[\mu_3\text{-}GeFeCp(CO)_2]_2$	2.73(1)					12j
$Fe_3(CO)_9[\mu_3\text{-}GeRe(CO)_5]_2$	2.719(4)					12i
$Fe_3(CO)_9[\mu_3\text{-}GeCo(CO)_4]_2$	2.753(6)					12h
$Fe_3(CO)_9[\mu_3\text{-}SnRe(CO)_5]_2$	2.807(4)					12l
$Fe_3(CO)_9[\mu_3\text{-}SnFeCp(CO)_2]_2$	2.792(6)					12k
$Fe_3(CO)_9[\mu_3\text{-}SnMn(CO)_5]_2$[g]	2.81					12m
$Fe_3(CO)_9[\mu_3\text{-}PCr(CO)_5]_2$	2.616(6)					17c
$Fe_3(CO)_9[\mu_3\text{-}PMnCp(CO)_2]_2$	2.636(6)					17c
$Fe_3(CO)_9(\mu_3\text{-}As)_2$	2.623(4)					17a
$Fe_3(CO)_9[\mu_3\text{-}AsCr(CO)_5]_2$	2.688(2)					17c
$Fe_3(CO)_9[\mu_3\text{-}AsMnCp(CO)_2]_2$	2.693(2)					17c
$Fe_3(CO)_9[\mu_3\text{-}SbCr(CO)_5]_2$	2.782(2)					17c
$Fe_3(CO)_9[\mu_3\text{-}SbMnCp(CO)_2]_2$	2.768(2)					17c
$Fe_3(CO)_9(\mu_3\text{-}Bi)_2$	2.75(1)					17b
$[PtRu_5(CO)_{15}(\mu\text{-}PbPh_2)(\mu_6\text{-}C)]$					2.6668(5)	13a
$Ru(CO)_2(PbPh_3)(^i\text{Pr-DAB})Cl$					2.7028(8)	13b
$[Ru_3\{\mu\text{-}PbR_2\}_2(\mu\text{-}CO)(CO)_9]$[h]		2.92(6)			2.78(1)	13c
$Ru_3(CO)_9(\mu_3\text{-}Bi)_2$		2.940(7)				19a
$Ru_3(CO)_9[\mu_3\text{-}GeRu(CO)_2(\eta^5\text{-}C_5Me_4H)]_2$		2.90(3)				19b
$Ru_3(CO)_{12}$		2.854(5)				20

[a] This work. [b] Pb−Cr(CO)$_4$. [c] Pb−Cr(CO)$_5$. [d] Equatorial. [e] Terminal. [f] FcN = $[Fe(\eta^5\text{-}C_5H_5)(\eta^5\text{-}C_5H_3(CH_2NMe_2)\text{-}2)\text{-}C,N]$. [g] Estimated standard deviations are not reported. [h] R = $CH(SiMe_3)_2$.

Scheme 2

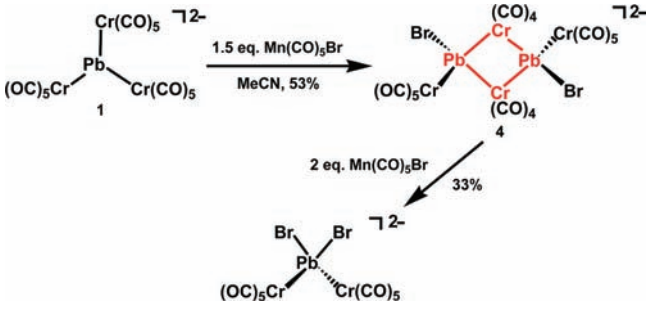

KOH/MeOH solution. Conversely, cluster **6** could be reconverted to **5** upon its reaction with $Fe(CO)_5$/KOH/MeOH. The DFT calculations also supported the observation that these transformations were reversible (discussed later).

The ORTEP diagram of cluster **5** is illustrated in Figure 3. The anion lies on a site that includes two crystallographic mirror planes, one going through the equatorial Fe_3 plane and the other including apical PbFe(CO) fragments and bisecting this plane. There is disorder across the latter plane, leading to 50% occupancy for each equatorial Fe atom that brings out two related orientation Fe_3 triangles by rotation of ca. 32° (see Figure S1 in the Supporting Information). Moreover, C8 and C8′, which are coordinated to the Fe4 atom, are disordered with 35% occupancy and 15% for C8a and C8a′. Further, the O8 and O8a aoms are also disordered, with 50% occupancy. The related trigonal-bipyramidal clusters $[Fe_3(\mu_3\text{-}CF)_2(CO)_9]$,[12g] $[Fe_3\{\mu_3\text{-}GeCo(CO)_4\}_2(CO)_9]$,[12h] $[Fe_3(\mu_3\text{-}As)_2(CO)_9]$,[17a] and $[Fe_3(\mu_3\text{-}Bi)_2(CO)_9]$[17b] crystallized in the higher-symmetry space group and showed similar disorder. Thus, cluster **5** exhibits the expected near-equilateral triangle of Fe atoms with both sides capped by Pb atoms, in which each Pb is further bonded to an $Fe(CO)_4$ group in a distorted tetrahedral environment and each Fe atom in the trigonal plane is bonded to three CO ligands.

Cluster **6** is isoelectronic and structurally similar to **5**, which consists of an equatorial $Fe_3(CO)_9$ triangular cluster with both sides capped by the $PbCr(CO)_5$ fragments (Figure 4). In accordance with the electron-counting rule,[18] three Fe−Fe bonds are observed for a 48-electron Fe_3-based cluster in both **5** and **6**. The average Pb−Fe(equatorial) bond of **5** [2.60(1) Å] is slightly shorter than that in **6** [2.65(3) Å], whereas the average Fe−Fe bond of **5** [2.83(4) Å] is comparable to that in **6** [2.79(6) Å],

(17) (a) Delbaere, L. T. J.; Kruczynski, L. J.; McBride, D. W. *J. Chem. Soc., Dalton Trans.* **1973**, 307–310. (b) Churchill, M. R.; Fettinger, J. C.; Whitmire, K. H. *J. Organomet. Chem.* **1985**, *284*, 13–23. (c) Collins, B. E.; Koide, Y.; Schauer, C. K.; White, P. S. *Inorg. Chem.* **1997**, *36*, 6172–6183. (d) Koide, Y.; Bautista, M. T.; White, P. S.; Schauer, C. K. *Inorg. Chem.* **1992**, *31*, 3690–3692. (e) Lang, H.; Huttner, G.; Zsolnai, L.; Mohr, G.; Sigwarth, B.; Weber, U.; Orama, O.; Jibril, I. *J. Organomet. Chem.* **1986**, *304*, 157–179. (f) Whitmire, K. H.; Shieh, M.; Lagrone, C. B.; Robinson, B. H.; Churchill, M. R.; Fettinger, J. C.; See, R. F. *Inorg. Chem.* **1987**, *26*, 2798–2807.

(18) (a) Mingos, D. M. P. *Acc. Chem. Res.* **1984**, *17*, 311–319. (b) Wade, K. *Adv. Inorg. Chem. Radiochem.* **1976**, *18*, 1–66.

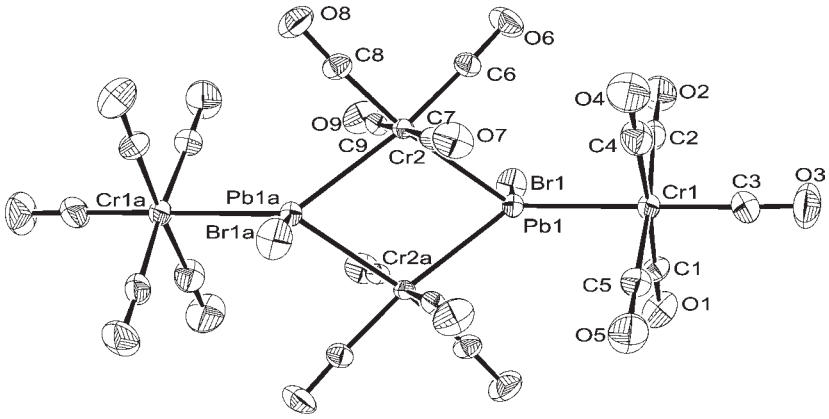

Figure 2. ORTEP diagram of anion **4**, showing 30% probability thermal ellipsoids. Selected bond lengths (Å) and angles (deg): Pb1−Cr1 2.679(2), Pb1−Cr2 2.732(2), Pb1−Br1 2.724(2), Pb1−Cr2a 2.716(2); Cr1−Pb1−Cr2 133.89(6), Cr1−Pb1−Cr2a 135.81(6), Cr2−Pb1−Cr2a 70.21(5), Cr1−Pb1−Br1 102.40(6), Cr2−Pb1−Br1 103.61(5), Cr2a−Pb1−Br1 105.66(5), Pb1−Cr2−Pb1a 109.79(5).

Scheme 3

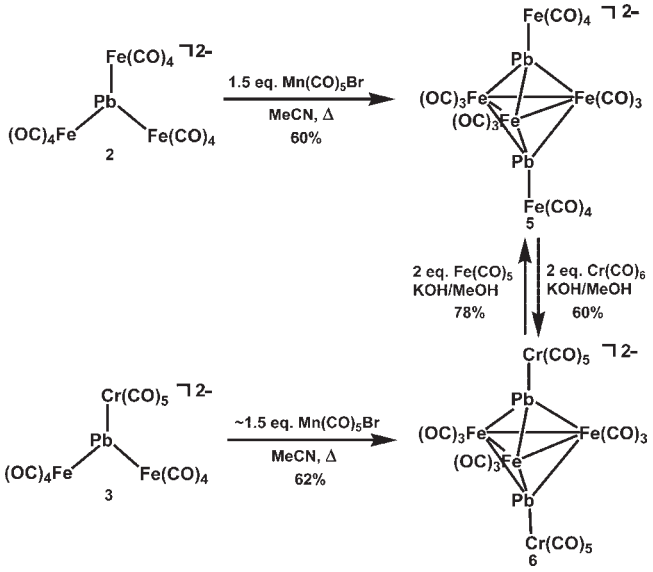

probably because of the lower steric hindrance of $Fe(CO)_4$ versus $Cr(CO)_5$ groups bonded to the Pb atoms (Table 1). The average Fe(terminal)−Pb−Fe(equatorial) and Fe(equatorial)−Pb−Fe(equatorial) angles of **5** are 140.99 and 66.02°, respectively. In **6**, the average Cr(terminal)−Pb−Fe(equatorial) and Fe(equatorial)−Pb−Fe(equatorial) angles are 142.43 and 63.51°, respectively. Although analogous E_2Fe_3 trigonal-bipyramidal clusters with E = C, Si, Ge, Sn, P, As, Sb, and Bi are known,[12g−m,17] clusters **5** and **6** represent the first Pb-capped Fe_3 examples. As shown in Table 1, the average Fe−Fe bonds in **5** [2.83(4) Å] and **6** [2.79(6) Å] are longer than those in the related clusters because of the larger size of the main-group Pb atom.

A more interesting finding was that the reaction of $PbCl_2$ with $Cr(CO)_6$ in a KOH/MeOH solution followed by the addition of $Ru_3(CO)_{12}$ could directly yield the lead-containing mixed chromium−ruthenium trigonal-bipyramidal complex $[Ru_3(CO)_9\{PbCr(CO)_5\}_2]^{2-}$ (**7**), which was isolated as the salt $[Et_4N]^+$ (Scheme 4). Unlike the mixed chromium−iron−lead cluster **3**, the analogous chromium−ruthenium−lead trigonal-planar complex $[Pb\{Cr(CO)_5\}\{Ru(CO)_4\}_2\}]^{2-}$ was not observable under similar reaction conditions, probably because of the reactive nature of the Pb−Ru bond (discussed later).

Cluster **7** is fully structurally characterized by spectroscopic methods, elemental analysis, and single-crystal X-ray diffraction. A diagram of the dianion **7** is shown in Figure 5. Cluster **7** is an analogue of **5** and **6**, with the core geometry based on a trigonal-bipyramidal arrangement of three equatorial $Ru(CO)_3$ groups and two axial $PbCr(CO)_5$ units. The average Cr(terminal)−Pb−Ru(equatorial) and Ru(equatorial)−Pb−Ru(equatorial) angles are 141.54 and 64.88°, respectively. As shown in Table 1, the average Pb−Cr length of **7** [2.680(4) Å] is close to that in **6** [2.67(1) Å], whereas the average Pb−Ru length of **7** [2.77(2) Å] is within the range of those in the reported compounds $[PtRu_5(CO)_{15}(\mu\text{-}PbPh_2)(\mu_6\text{-}C)]$ [2.6668(5) Å],[13a] $[Ru(CO)_2(PbPh_3)(^i\text{Pr-DAB})Cl]$ [2.7028(8) Å],[13b] and $[Ru_3\{\mu\text{-}PbR_2\}_2(\mu\text{-}CO)(CO)_9]$ [2.78(1) Å, R = $CH(SiMe_3)_2$].[13c] Moreover, the average Ru−Ru distance of **7** is 2.97(1) Å, a bit longer than those in the related Ru_3 clusters $[Ru_3(CO)_9(\mu_3\text{-}Bi)_2]$ [2.940(7) Å],[19a] $Ru_3(CO)_9[\mu_3\text{-}GeRu(CO)_2(\eta^5\text{-}C_5Me_4H)]_2$ [2.90(3) Å],[19b] and $Ru_3(CO)_{12}$ [2.854(5) Å],[20] indicative of the small effect of the apical atoms. A search of the Cambridge Crystallographic Data Centre failed to yield any structurally characterized compounds with the Cr−Pb−Fe or Cr−Pb−Ru fragment. Clusters **6** and **7** represent the first examples of lead-containing mixed chromium and group 8 clusters.

DFT Calculations. The computational method of DFT was employed in an attempt to better understand the nature of complexes **1**−**7**. These calculations were carried out using the B3LYP DFT method[21,22] with LanL2DZ/6-31G(d) basis sets. The geometries of the X-ray-determined and proposed intermediates in this study were fully optimized, and the natural bond order (NBO)[23] and natural population analyses (NPA)[24] for complexes **1**−**7** are displayed in Table 2.

(19) (a) Hay, C. M.; Johnson, B. F. G.; Lewis, J.; Raithby, P. R.; Whitton, A. J. *J. Chem. Soc., Dalton Trans.* **1988**, 2091–2097. (b) Zhang, Y.; Wang, B.; Xu, S.; Zhou, X. *Organometallics* **2001**, *20*, 3829–3832.
(20) Churchill, M. R.; Hollander, F. J.; Hutchinson, J. P. *Inorg. Chem.* **1977**, *16*, 2655–2659.
(21) (a) Becke, A. D. *J. Chem. Phys.* **1993**, *98*, 5648–5652. (b) Becke, A. D. *J. Chem. Phys.* **1992**, *96*, 2155–2160. (c) Becke, A. D. *J. Chem. Phys.* **1992**, *97*, 9173–9177.
(22) Lee, C.; Yang, W.; Parr, R. G. *Phys. Rev. B* **1988**, *B37*, 785–789.
(23) Reed, A. E.; Curtiss, L. A.; Weinhold, F. *Chem. Rev.* **1988**, *88*, 899–926.
(24) (a) Reed, A. E.; Weinhold, F. *J. Chem. Phys.* **1983**, *78*, 4066–4073. (b) Reed, A. E.; Weinstock, R. B.; Weinhold, F. *J. Chem. Phys.* **1985**, *83*, 735–746.

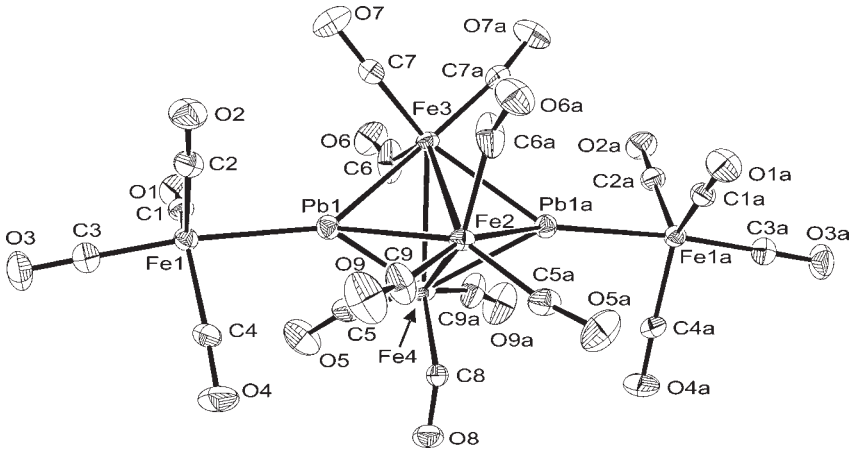

Figure 3. ORTEP diagram of anion **5**, showing 30% probability thermal ellipsoids. Selected bond lengths (Å) and angles (deg): Pb1−Fe1 2.546(1), Pb1−Fe2 2.609(2), Pb1−Fe3 2.588(2), Pb1−Fe4 2.598(2), Fe2−Fe3 2.812(3), Fe3−Fe4 2.805(4), Fe4−Fe2 2.875(4); Fe3−Fe2−Fe4 59.10(9), Fe2−Fe3−Fe4 61.6(1), Fe2−Fe4−Fe3 59.33(8).

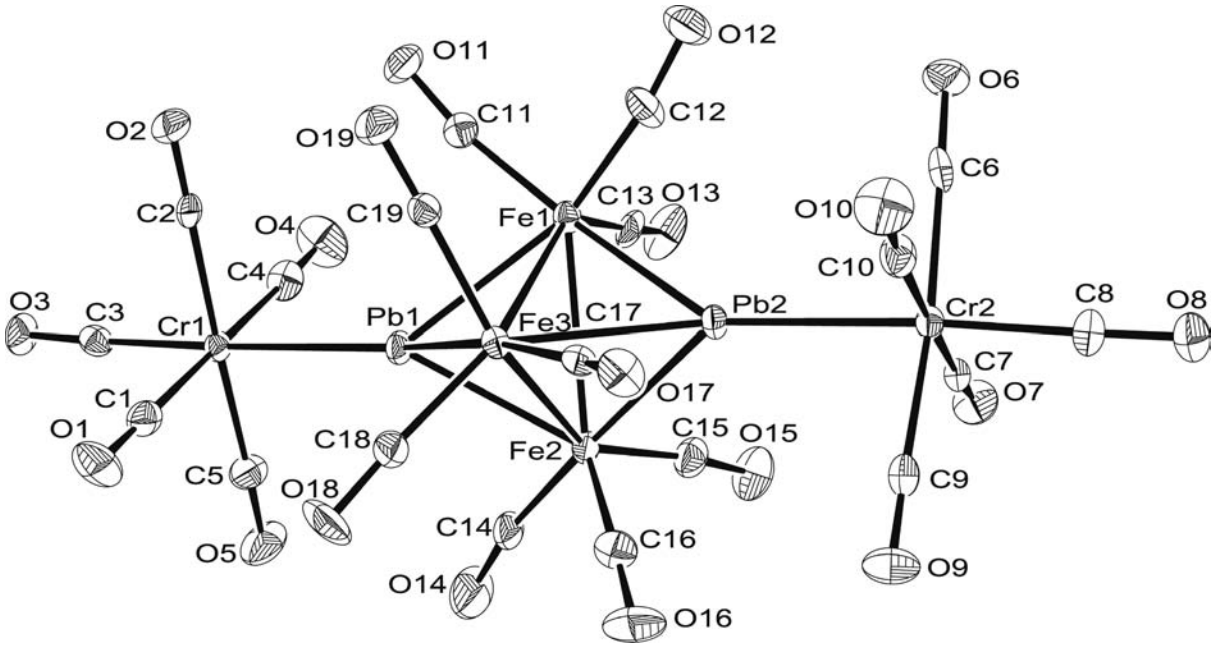

Figure 4. ORTEP diagram of anion **6**, showing 30% probability thermal ellipsoids. Selected bond lengths (Å) and angles (deg): Pb1−Fe1 2.653(1), Pb1−Fe2 2.640(1), Pb1−Fe3 2.661(1), Pb1−Cr1 2.684(1), Pb2−Fe1 2.611(1), Pb2−Fe2 2.626(1), Pb2−Fe3 2.699(1), Pb2−Cr2 2.664(1), Fe1−Fe2 2.859(2), Fe2−Fe3 2.748(2), Fe3−Fe1 2.754(2); Fe1−Fe2−Fe3 58.78(4), Fe2−Fe3−Fe1 62.63(5), Fe3−Fe1−Fe2 58.59(4).

Scheme 4

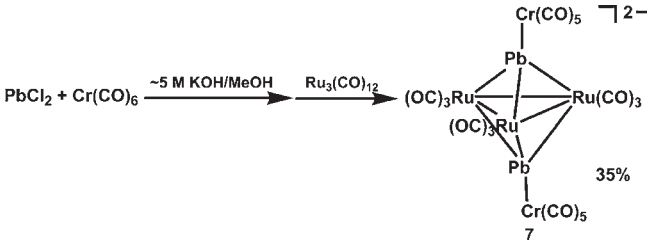

The calculation showed that the active sites of complexes **1**−**3** for the formation of complexes **4**−**6** could be related to the frontier orbitals of complexes **1**−**3**. As shown in Figure 6, the lowest unoccupied molecular orbital (LUMO) and LUMO+1 of complexes **1**−**3** had a significant contribution from the p_z or s orbital of the Pb atom, with almost the same energy. It was noted that the LUMO of complex **1** was similar to the LUMO+1 of **2** and **3**, while the LUMO+1 of complex **1** was similar to the LUMOs of complexes **2** and **3**. Thus, it was reasonable to propose that the incoming Br^- could interact with the Pb atom of complex **1** first, accompanied by a further coupling reaction to give rise to complex **4**. This process also postulated that Br^- attacked the positively charged Pb atom (+0.646) of **1** followed by the loss of $[Cr(CO)_5]^{2-}$ to give the proposed intermediate "$[BrPb\{Cr(CO)_5\}_2]^-$", where the negatively charged Cr atom (−1.443) further interacted with the Pb atom (+0.917) of another molecule of the intermediate, accompanied by the release of CO units to give the dimeric product (Scheme 5). This assumption was supported by the fact that the As center of the isoelectronic $ClAs\{Cr(CO)_5\}_2$ was susceptible to nucleophilic species.[25] Further reaction

(25) von Seyerl, J.; Huttner, G. *Angew. Chem., Int. Ed. Engl.* **1979**, *18*, 233–234.

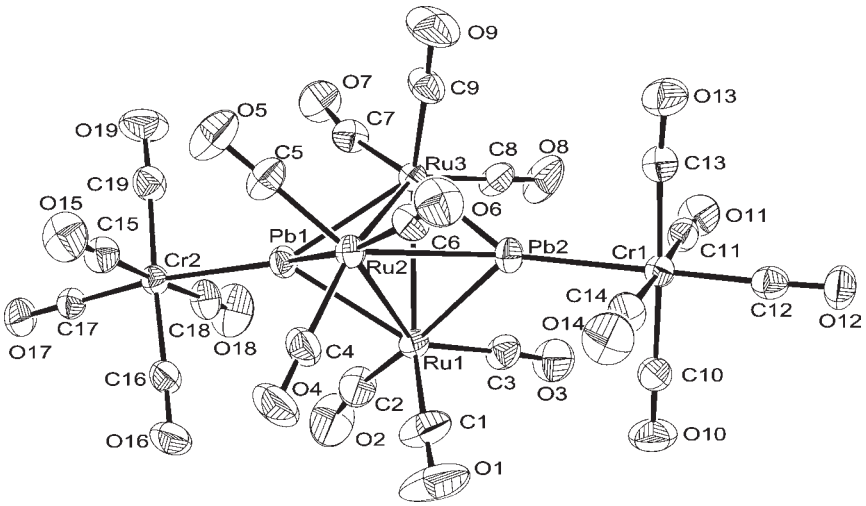

Figure 5. ORTEP diagram of anion **7**, showing 30% probability thermal ellipsoids. Selected bond lengths (Å) and angles (deg): Pb1−Ru1 2.7715(6), Pb1−Ru2 2.7452(6), Pb1−Ru3 2.7809(6), Pb1−Cr2 2.682(1), Pb2−Ru1 2.7458(6), Pb2−Ru2 2.8020(6), Pb2−Ru3 2.7594(6), Pb2−Cr1 2.677(1), Ru1−Ru2 2.9805(8), Ru2−Ru3 2.9526(8), Ru3−Ru1 2.9744(8); Ru1−Ru2−Ru3 60.17(2), Ru2−Ru3−Ru1 60.38(2), Ru3−Ru1−Ru2 59.45(2).

Table 2. Results of NBO and NPA of Complexes **1**−**7**, the Proposed Intermediates $[BrPb\{Cr(CO)_5\}_2]^-$ and $[Pb\{Cr(CO)_5\}\{Ru(CO)_4\}_2]^{2-}$, and $Ru_3(CO)_{12}$

	Wiberg bond index					natural charge			
complex	Pb−Cr	Pb−Fe	Pb−Ru	Pb−M_{eq}	M_{eq}−M_{eq}	Pb	Cr	Fe	Ru
1	0.317					0.646	−1.401		
2		0.313				0.619		−0.554	
3	0.302	0.321				0.619	−1.389	−0.555	
$[BrPb\{Cr(CO)_5\}_2]^-$	0.385					0.917	−1.443		
4	0.258[a]					0.763	−1.068[a]		
	0.377[b]						−1.424[b]		
5		0.340		0.270	0.131	0.492		−0.469[a]	
								−0.530[b]	
6	0.326			0.278	0.127	0.463	−1.374	−0.455	
7	0.328			0.287	0.112	0.320	−1.379		−0.406
$[Pb\{Cr(CO)_5\}\{Ru(CO)_4\}_2]^{2-}$	0.310		0.277			0.576	−1.389		−0.325
$Ru_3(CO)_{12}$					0.193				−0.342

[a] Ring. [b] Terminal.

of complex **4** with $Mn(CO)_5Br$ also involved the attack of Br^- on the positively charged Pb atom (+0.763) of **4**, with Pb−Cr bond cleavage. In addition, the calculated Wiberg bond indices (also called the bond orders) of complex **4** reflected a weak Pb−$Cr(CO)_4$ bond, which could have facilitated further Br^- attacks on Pb atoms, leading to the formation of the known complex $[PbBr_2Cr_2(CO)_{10}]^{2-}$ (Table 2).[11b]

The formation of the trigonal-bipyramidal clusters **5** and **6** from the trigonal-planar complexes **2** and **3**, respectively, was then examined. The highest occupied molecular orbital (HOMO) and HOMO−1 of complex **2** were nearly degenerate with the significant contributions from the p and d orbitals of the Fe atoms (Figure 6). It was also found that the HOMO of **2** was similar to the HOMO−1 of **3**, while the HOMO−1 of **2** was similar to the HOMO of complex **3**. As mentioned above, the LUMO and LUMO+1 of complexes **2** and **3** were also close in energy with the significant contribution from the s or p_z orbital of the Pb atom (Figure 6). Therefore, it is reasonable to suggest that the negatively charged Fe atom of complex **2** (−0.554) or **3** (−0.555) underwent nucleophilic attack on the positively charged Pb atom of another molecule of complex **2** (+0.619) or **3** (+0.619), with Pb−Fe and Fe−Fe bond formation and the loss of one $[Fe(CO)_4]^{2-}$ and three CO ligands. As shown in Table 2, it should be mentioned that the Pb atom in complexes **5** and **6** became less positively charged (+0.492 or +0.463) and the Fe atom became less negatively charged (−0.469, −0.530, or −0.455) compared to **2** and **3**, indicating the stronger covalent character of the Pb−Fe bonds in **5** and **6**. Moreover, calculations gave $\Delta G = -5.502$ kcal/mol for the conversion of **5** to **6**, which supported the experimental results that the conversion was reversible upon the addition of $[Cr(CO)_5]^{2-}$ or $[Fe(CO)_4]^{2-}$ but was easier for the transformation of complex **5** to **6**. Further NPA showed that the Pb atom in **5** carried a positive charge of +0.492 and the Fe atom in the $Fe(CO)_4$ fragment carried a charge of −0.530, while the Pb atom in **6** carried a charge of +0.463 and the Cr atom in the $Cr(CO)_5$ group carried a negative charge of −1.374, suggestive of the larger coulomb attraction between the Pb atom and $Cr(CO)_5$ in cluster **6**.

The failure to observe the trigonal-planar intermediate $[Pb\{Cr(CO)_5\}\{Ru(CO)_4\}_2]^{2-}$ from the reaction of $PbCl_2$, $Cr(CO)_6$, and $Ru_3(CO)_{12}$ was probably because of weak Pb−Ru bonds. This phenomenon was supported by the calculation that the Wiberg bond index of the Pb−Ru bond (0.277) for the proposed intermediate "$[Pb\{Cr(CO)_5\}\{Ru(CO)_4\}_2]^{2-}$" was significantly smaller than those for the Pb−Cr (0.302−0.317) and Pb−Fe (0.313−0.321) bonds in the corresponding triangular-planar lead complexes

Scheme 5

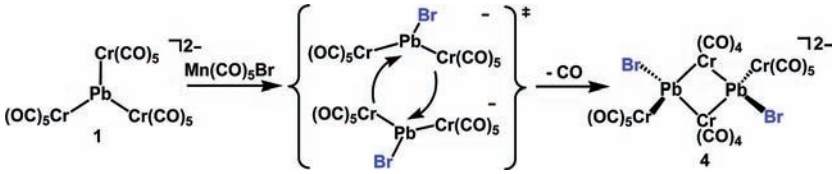

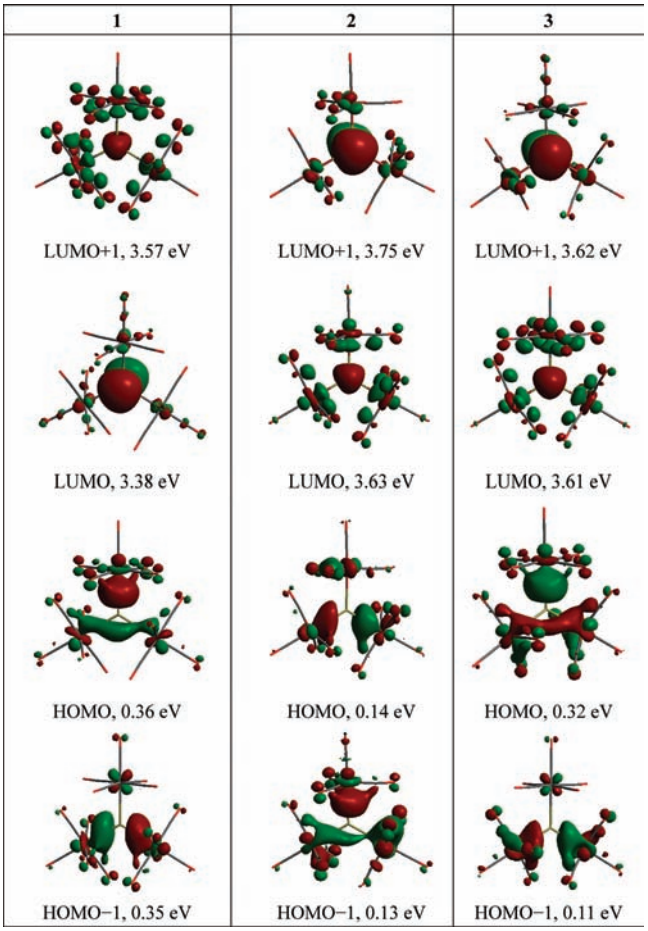

Figure 6. Spatial graphs (isovalue = 0.04−0.05) of the selected frontier molecular orbitals of complexes **1**−**3**.

1−**3**. In addition, the Wiberg bond index of the Ru−Ru bond in cluster **7** was 0.112, smaller than that in $Ru_3(CO)_{12}$ (0.193) but comparable to that (0.09) for $[\{PPh_4\}_2\{Te_2Ru_4(CO)_{10}Cu_4Br_2Cl_2\}\cdot THF]_\infty$ (THF = tetrahydrofuran) in the Te−Ru system.[9a]

Electrochemistry of 5−**7.** In view of the highly symmetric Pb_2M_3 (M = Fe, Ru) metal cores of the analogous complexes **5**−**7**, their electrochemical properties were investigated using cyclic voltammetry (CV) and differential pulse voltammetry (DPV) in MeCN under N_2, which could be further compared with the related clusters $M_3(CO)_{12}$ (M = Fe, Ru).[26] The electrochemical data for each complex studied are listed in Tables 3 and S1 in the Supporting Information.

The cyclic voltammograms of Fe_3Pb_2 trigonal-bipyramidal clusters **5** and **6** exhibited three quasi-reversible reductions (around −1.31 to −2.21 V), in which some of

(26) Bond, A. M.; Dawson, P. A.; Peake, B. M.; Robinson, B. H.; Simpson, J. *Inorg. Chem.* **1977**, *16*, 2199–2206.

Table 3. DPV of **5**−**7**, $Fe_3(CO)_{12}$, and $Ru_3(CO)_{12}$

complex	reduction process E_p^{red}/V[a] ($W_{1/2}$/mV[b])		
5	−1.238 (107)	−1.550 (171)	−2.102 (110)
6	−1.430 (97)	−1.694 (150)	−2.074 (93)
$Fe_3(CO)_{12}$	−0.440 (92)	−0.904 (200)	−2.028 (120)
7	−1.748 (132)	−2.016 (88)	−2.244 (150)
$Ru_3(CO)_{12}$	−0.898 (−)[c]	−1.106 (160)	−2.078 (104)

[a] E_p^{red} = reductive peak potential. [b] $W_{1/2}$ = width at half-height. [c] Difficult to determine.

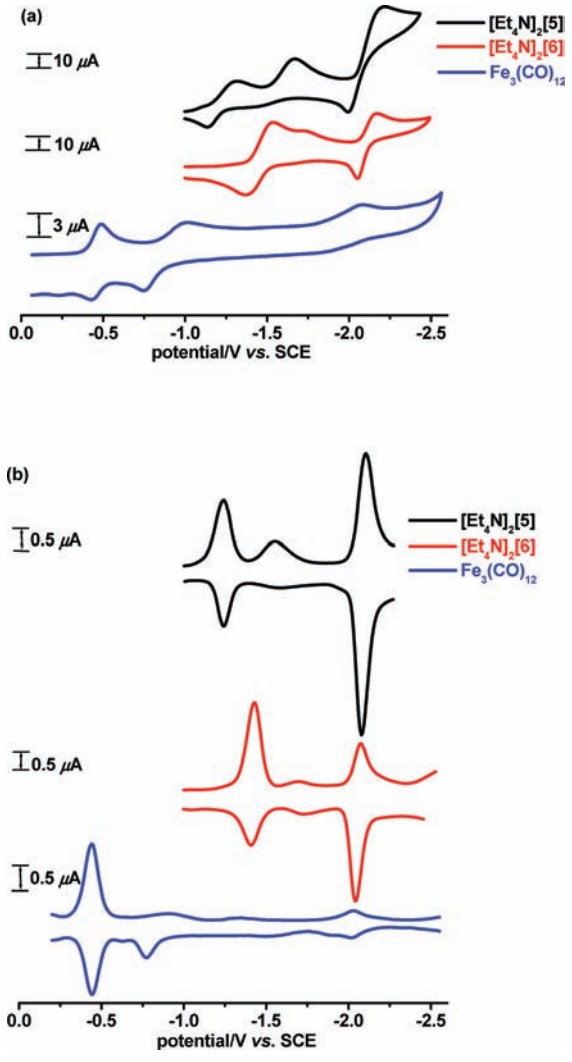

Figure 7. CV (a) and DPV (b) in MeCN for $[Et_4N]_2$[**5**], $[Et_4N]_2$[**6**], and $Fe_3(CO)_{12}$. Conditions: electrolyte, 0.1 M Bu_4NClO_4; working electrode, glassy carbon; scan rate, 100 mV/s. Potentials are versus SCE.

the peaks were unresolved (Figure 7a). Further DPV results revealed that **5** and **6** each had three quasi-reversible redox reductions at −1.238, −1.550, and −2.102 V and at −1.430, −1.694, and −2.074 V, respectively (Figure 7b). In light of

Table 4. Reduction Potentials and Electronic Affinities of Complexes **5**−**7**

complex	reduction potential E^a (V)	EA^b (kcal/mol)
5	−1.238	78.13
6	−1.430	81.57
7	−1.748	86.09

^{a} From DPV. ^{b} The EA can be estimated by EA ≈ $E_{elec}(N+1) - E_{elec}(N)$, where $E_{elec}(N+1)$ and $E_{elec}(N)$ represent the electronic energies of molecules with $N + 1$ and N electrons, respectively.[27]

the DFT calculations, the LUMO contributions of **5** and **6** predominantly came from the p and d orbitals of the equatorial Fe_3 moieties, indicating that the reduction processes of **5** and **6** occurred in the triangular $Fe_3(CO)_9$ ring (Figure S2 in the Supporting Information). The results suggested that complexes **5** and **6** $[[Fe_3(CO)_9\{PbM(CO)_x\}_2]^{2-}$ (M = Fe, x = 4, **5**; M = Cr, x = 5, **6**)] could be reduced to form the square-pyramidal complexes $[Fe_3(CO)_9\{PbM(CO)_x\}_2]^{4-}$, with Fe−Fe bond breakage, which paralleled the chemistry of $[Fe_3(\mu_3\text{-}Bi)_2(CO)_9]$.[17f] As shown in Figure 7b, $Fe_3(CO)_{12}$ revealed a similar pattern of three redox couples at −0.440, −0.904, and −2.028 V. Compared with $Fe_3(CO)_{12}$, the reduction potentials of clusters **5** and **6** were shifted to more negative values, basically because of the negative charges of the complexes. Furthermore, the first quasi-reversible reduction of complex **6** (−1.430 V) revealed a significant cathodic shift, in contrast with complex **5** (−1.238 V), because of the larger electron-donating ability of the apical $Cr(CO)_5$ versus $Fe(CO)_4$ fragments. This result was also supported by calculations that indicated that complex **6** had a smaller electron affinity, compared with complex **5** [EA ≈ $E_{elec}(N+1) - E_{elec}(N)$,[27] 81.57 vs 78.13 kcal/mol; Table 4].

On the other hand, as shown in Figure 8, the DPV study of the Ru_3Pb_2 trigonal-bipyramidal cluster **7** exhibited three quasi-reversible reductions (−1.748, −2.016, and −2.244 V) that should have occurred around the equatorial $Ru_3(CO)_9$ ring, in view of the major contribution of the LUMO from the triangular ruthenium moiety (Figure S2 in the Supporting Information). Similar to the case for the Fe_3Pb_2 trigonal-bipyramidal clusters **5** and **6**, the Ru_3Pb_2 complex **7** also showed significant cathodic shifts compared with those of $Ru_3(CO)_{12}$. Moreover, the first quasi-reversible reduction of **7** (−1.748 V) versus **6** (−1.430 V) revealed that **7** was more difficult to reduce than the isostructural cluster **6**, which is also supported by the smaller electron affinity calculated for **7** compared with **6** (Table 4).

Conclusion

The facile synthesis of the first examples of mixed-metal carbonyl lead-containing trigonal-planar complex **3** and trigonal-bipyramidal clusters $[M_3(CO)_9\{PbCr(CO)_5\}_2]^{2-}$ (M = Fe, Ru) was demonstrated. The nature, formation, and structural transformation of these new complexes were systematically described and compared in terms of the characteristics of transition metals. In addition, three Fe_3Pb_2- or Ru_3Pb_2-based trigonal-bipyramidal closo clusters demonstrated a wide range of quasi-reversible redox ability. More interestingly, pronounced cathodic shifts were observed from the Fe_3 to the Ru_3 ring or as the apical fragment changed from an $Fe(CO)_4$ fragment to a $Cr(CO)_5$ fragment, which was illustrated well by the results of DFT calculations. This study provides a new avenue to a systematic comparison of the complicated electronic effects of mixed-metal clusters on the basis of electrochemical and theoretical studies.

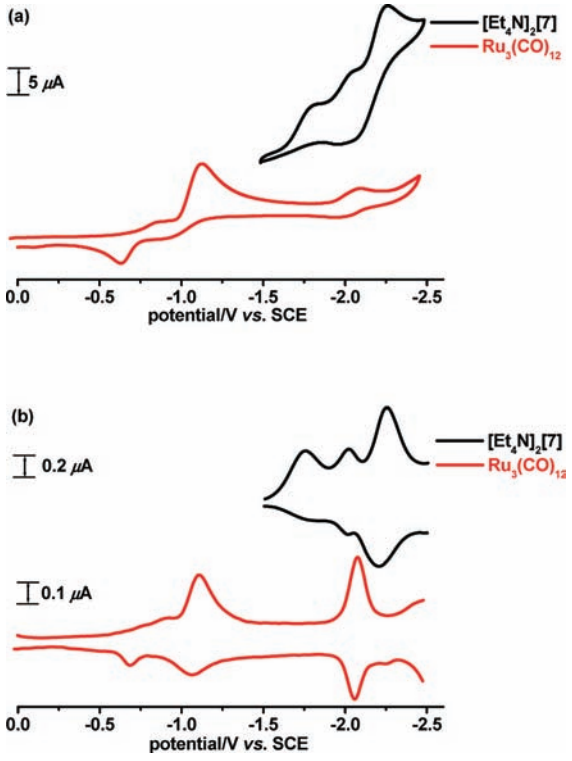

Figure 8. CV (a) and DPV (b) in MeCN for $[Et_4N]_2$[**7**] and $Ru_3(CO)_{12}$. Conditions: electrolyte, 0.1 M Bu_4NClO_4; working electrode, glassy carbon; scan rate, 100 mV/s. Potentials are versus SCE.

Experimental Section

All reactions were performed under an atmosphere of pure nitrogen using standard Schlenk techniques.[28] Solvents were purified, dried, and distilled under nitrogen prior to use. $Cr(CO)_6$ (Strem), $Fe(CO)_5$ (Strem), $Ru_3(CO)_{12}$ (Strem), $Mn(CO)_5Br$ (Strem), $PbCl_2$ (Osaka), and KOH (Showa) were used as received. The compound $[Et_4N]_2[Pb\{Fe(CO)_4\}_3]$ ($[Et_4N]_2$[**2**]) was prepared according to the published method.[12a] IR spectra were recorded on a Perkin-Elmer Paragon 500 IR spectrometer as solutions in CaF_2 cells. Elemental analyses for C, H, and N were performed on a Perkin-Elmer 2400 analyzer at the NSC Regional Instrumental Center at National Taiwan University, Taipei, Taiwan. Electrochemical measurements were performed at room temperature under a nitrogen atmosphere and recorded using a BAS-100W electrochemical potentiostat. A glassy carbon working electrode, a platinum wire auxiliary electrode, and a nonaqueous Ag/Ag^+ electrode were used in a three-electrode configuration. Tetra-*n*-butylammonium perchlorate was used as the supporting electrolyte, and the solute concentration was ~10^{-3} M. The redox potentials were calibrated with a ferrocenium/ferrocene (Fc^+/Fc) couple in the working solution and referenced to a saturated calomel electrode (SCE).

Synthesis of $[Et_4N]_2[Pb\{Cr(CO)_5\}_3]$ ($[Et_4N]_2$[1]). To a MeOH solution (15 mL) of $Cr(CO)_6$ (0.68 g, 3.09 mmol) and KOH (4.21 g, 75.0 mmol) was added $PbCl_2$ (0.28 g, 1.01 mmol) in an ice/water bath. The resulting solution was stirred at ambient temperature for 4 h to give a reddish-brown solution. The solution was filtered and concentrated, and a MeOH solution of $[Et_4N]Br$ (0.35 g,

(27) Lin, Y.-l.; Lee, Y.-m.; Lim, C. *J. Am. Chem. Soc.* **2005**, *127*, 11336–11347.

(28) Shriver, D. F.; Drezdon, M. A. *The Manipulation of Air-Sensitive Compounds*; Wiley-VCH Publishers: New York, 1986.

Table 5. Crystallographic Data for $[Bu_4N]_2$[**3**], $[Et_4N]_2$[**4**], $[Et_4N]_2$[**5**], $[Et_4N]_2$[**6**], and $[Et_4N]_2$[**7**]

	$[Bu_4N]_2$[**3**]	$[Et_4N]_2$[**4**]	$[Et_4N]_2$[**5**]	$[Et_4N]_2$[**6**]	$[Et_4N]_2$[**7**]
empirical formula	$C_{45}H_{72}CrFe_2N_2O_{13}Pb$	$C_{34}H_{40}Br_2Cr_4N_2O_{18}Pb_2$	$C_{33}H_{40}Fe_5N_2O_{17}Pb_2$	$C_{35}H_{40}Cr_2Fe_3N_2O_{19}Pb_2$	$C_{35}H_{40}Cr_2Ru_3N_2O_{19}Pb_2$
fw	1219.94	1546.89	1430.30	1478.62	1614.31
cryst syst	monoclinic	monoclinic	monoclinic	monoclinic	monoclinic
space group	$P2_1/n$	$P2_1/c$	$C2/c$	$P2_1/c$	$P2_1/n$
crystal dimens, mm	0.40 × 0.25 × 0.20	0.40 × 0.05 × 0.03	0.41 × 0.24 × 0.07	0.25 × 0.22 × 0.18	0.20 × 0.12 × 0.10
a, Å	12.281(3)	9.5681(2)	28.3677(6)	12.9995(2)	12.1695(1)
b, Å	33.391(1)	24.6016(6)	10.6192(3)	18.8599(3)	18.2147(3)
c, Å	13.865(4)	11.3668(3)	17.6363(4)	20.5628(4)	23.5738(3)
α, deg					
β, deg	90.32(2)	101.805(1)	120.414(2)	107.506(1)	103.0966(6)
γ, deg					
V, Å^3	5686(3)	2619.1(1)	4581.7(2)	4807.9(1)	5089.5(1)
Z	4	2	4	4	4
D(calcd), g/cm^3	1.425	2.007	2.074	2.043	2.107
μ, mm^{-1}	3.692	8.799	8.926	8.362	7.935
color, habit	black, prism	black, prism	black, prism	black, prism	red, prism
diffractometer	Nonius (CAD4)	Nonius (Kappa CCD)	Nonius (Kappa CCD)	Nonius (Kappa CCD)	Nonius (Kappa CCD)
radiation (λ), Å	0.710 73	0.710 73	0.710 73	0.710 73	0.710 73
temp, K	298	298	200	298	298
θ range for data collcn, deg	1.59−24.92	3.53−27.71	2.09−25.33	2.08−25.34	4.10−27.47
T_{min}/T_{max}	0.32/0.53	0.30/0.41	0.12/0.57	0.17/0.20	0.29/0.39
no. of indep reflns [$I > 2\sigma(I)$]	4646 (R_{int} = 0.0633)	4481 (R_{int} = 0.0928)	3521 (R_{int} = 0.0798)	6745 (R_{int} = 0.0747)	7441 (R_{int} = 0.0690)
no. of param	572	280	286	568	568
R1[a]/wR2[a] [$I > 2\sigma(I)$]	0.060/0.138	0.071/0.172	0.057/0.144	0.042/0.106	0.045/0.082
R1[a]/wR2[a] (all data)	0.165/0.179	0.095/0.184	0.072/0.165	0.068/0.140	0.089/0.094

[a] The functions minimized during least-squares cycles were $R1 = \sum||F_o| - |F_c||/\sum|F_o|$ and $wR2 = [\sum[w(F_o^2 - F_c^2)^2]/\sum[w(F_o^2)^2]]^{1/2}$.

1.67 mmol) was added dropwise, precipitating the solid. The solid was washed with deionized water in an ice/water bath several times and dried under vacuum. The THF extract was recrystallized from Et_2O/THF to give a reddish-brown sample of $[Et_4N]_2$[**1**] (yield 0.29 g, 0.28 mmol, 28% based on $PbCl_2$). IR (ν_{CO}, THF): 2010 (w), 1977 (s), 1909 (vs), 1864 (m) cm^{-1}.

Synthesis of $[Bu_4N]_2[Pb\{Cr(CO)_5\}\{Fe(CO)_4\}_2]$ ($[Bu_4N]_2$[3]). A MeOH solution (20 mL) of $PbCl_2$ (0.77 g, 2.77 mmol), $Cr(CO)_6$ (0.61 g, 2.77 mmol), and KOH (5.20 g, 92.7 mmol) was stirred in an ice/water bath. The solution was stirred at ambient temperature for 2 h, and $Fe(CO)_5$ (0.73 mL, 5.55 mmol) was added. The reaction solution turned brown and was allowed to stir for 12 h. The resulting solution was filtered and concentrated, and an aqueous solution of $[Bu_4N]Br$ (0.70 g, 2.17 mmol) was added dropwise, precipitating the solid. The solid was washed with deionized water several times and dried under vacuum. The THF extract was recrystallized from Et_2O/THF to give a reddish-brown sample of $[Bu_4N]_2$[**3**] (yield 1.12 g, 0.92 mmol, 33% based on $PbCl_2$). IR (ν_{CO}, THF): 2025 (m), 1972 (s), 1957 (vs), 1910 (s), 1878 (s) cm^{-1}. Anal. Calcd for $[Bu_4N]_2$[**3**]: C, 44.30; H, 5.95; N, 2.30. Found: C, 44.24; H, 6.19; N, 2.57. Crystals of $[Bu_4N]_2$[**3**] suitable for X-ray diffraction were grown from Et_2O/THF. $[Et_4N]_2$[**3**] can be isolated by following a similar procedure.

Reaction of $[Et_4N]_2$[1] with $Mn(CO)_5Br$. To a MeCN solution (30 mL) of $[Et_4N]_2$[**1**] (0.36 g, 0.34 mmol) was added $Mn(CO)_5Br$ (0.14 g, 0.51 mmol) at ambient temperature. The resulting solution was stirred for 30 min to give a yellow-brown solution. The solution was filtered, and the solvent was evaporated under vacuum. The residue was washed with Et_2O, which was shown to contain $Mn_2(CO)_{10}$ and $[HCr_2(CO)_{10}]^-$ by IR spectroscopy. The residue was extracted with CH_2Cl_2 to give a sample of $[Et_4N]_2[Pb_2Br_2Cr_4(CO)_{18}]$ ($[Et_4N]_2$[**4**]) (yield 0.14 g, 0.09 mmol, 53% based on Pb). IR (ν_{CO}, CH_2Cl_2): 2036 (s), 2012 (m), 1984 (s), 1959 (m), 1943 (m), 1925 (s), 1903 (m) cm^{-1}. Anal. Calcd for $[Et_4N]_2$[**4**]: C, 26.40; H, 2.61; N, 1.81. Found: C, 26.41; H, 2.80; N, 1.66. Crystals of $[Et_4N]_2$[**4**] suitable for single crystal X-ray diffraction were grown from Et_2O/CH_2Cl_2.

Reaction of $[Et_4N]_2$[4] with $Mn(CO)_5Br$. To a MeCN solution (10 mL) of $[Et_4N]_2[Pb_2Br_2Cr_4(CO)_{18}]$ ($[Et_4N]_2$[**4**]) (0.14 g, 0.09 mmol) was added $Mn(CO)_5Br$ (0.05 g, 0.18 mmol). The mixed solution was stirred at ambient temperature for 21 h. The solution was filtered, and the solvent was evaporated under vacuum. The residue was extracted with CH_2Cl_2 to give a sample of $[Et_4N]_2[PbBr_2Cr_2(CO)_{10}]$[11b] (yield 0.06 g, 0.06 mmol, 33% based on $[Et_4N]_2[Pb_2Br_2Cr_4(CO)_{18}]$). IR ($\nu_{CO}$, CH_2Cl_2): 1990 (m), 1953 (vs), 1893 (m), 1859 (m) cm^{-1}.

Synthesis of $[Et_4N]_2[Fe_3(CO)_9\{PbFe(CO)_4\}_2]$ ($[Et_4N]_2$[5]). Method 1. A MeCN solution (30 mL) of $[Et_4N]_2[Pb\{Fe(CO)_4\}_3]$ ($[Et_4N]_2$[**2**]) (2.02 g, 2.08 mmol) and $Mn(CO)_5Br$ (0.86 g, 3.13 mmol) was stirred and heated at 80 °C for 42 h. The resultant yellowish-brown solution was filtered, and the solvent was evaporated under vacuum. The residue was washed several times with deionized water and Et_2O, which was shown to contain $Mn_2(CO)_{10}$ by IR spectroscopy. The CH_2Cl_2 extract was recrystallized from Et_2O/MeOH/CH_2Cl_2 to give a sample of $[Et_4N]_2$[**5**] (yield 0.89 g, 0.62 mmol, 60% based on Pb). IR (ν_{CO}, CH_2Cl_2): 2011 (s), 1955 (vs), 1911 (m) cm^{-1}. Anal. Calcd for $[Et_4N]_2$[**5**]: C, 27.71; H, 2.82; N, 1.96. Found: C, 27.66; H, 2.49; N, 2.05. Crystals of $[Et_4N]_2$[**5**] suitable for single-crystal X-ray diffraction were grown from Et_2O/CH_2Cl_2.

Method 2. To a MeCN solution (20 mL) of $[Et_4N]_2[Fe_3(CO)_9\{PbCr(CO)_5\}_2]$ ($[Et_4N]_2$[**6**]) (0.61 g, 0.41 mmol) was added $Fe(CO)_5$ (0.11 mL, 0.84 mmol), KOH (4.14 g, 73.8 mmol), and MeOH (30 mL). The mixed solution was stirred at ambient temperature for 40 h. The solution was filtered, and the solvent was evaporated under vacuum. The residue was washed several times with Et_2O and extracted with CH_2Cl_2 to give a sample of $[Et_4N]_2$[**5**] (yield 0.46 g, 0.32 mmol, 78% based on Pb).

Synthesis of $[Et_4N]_2[Fe_3(CO)_9\{PbCr(CO)_5\}_2]$ ($[Et_4N]_2$[6]). Method 1. To a MeCN solution (40 mL) of $[Et_4N]_2$[**3**] (1.00 g, 1.00 mmol) was added $Mn(CO)_5Br$ (0.36 g, 1.31 mmol). The mixed solution was stirred and heated to 80 °C for 2 days. The solution was filtered, and the solvent was evaporated under vacuum. The residue was washed several times with Et_2O, which was shown by IR spectroscopy to contain $Mn_2(CO)_{10}$. The residue

was then extracted with CH_2Cl_2 to give a sample of $[Et_4N]_2$[**6**] (yield 0.46 g, 0.31 mmol, 62% based on Pb). IR (ν_{CO}, CH_2Cl_2): 2034 (s), 1949 (vs), 1918 (m), 1886 (m) cm^{-1}. Anal. Calcd for $[Et_4N]_2$[**6**]: C, 28.43; H, 2.73; N, 1.89. Found: C, 28.40; H, 2.81; N, 1.86. Crystals of $[Et_4N]_2$[**6**] suitable for single-crystal X-ray diffraction were grown from Et_2O/CH_2Cl_2.

Method 2. A MeOH solution (30 mL) of $Cr(CO)_6$ (0.10 g, 0.45 mmol) and KOH (4.23 g, 0.075 mmol) was stirred in an ice/water bath and warmed to ambient temperature. After 4 h, $[Et_4N]_2$[**5**] (0.29 g, 0.20 mmol) was added to the solution, which was stirred for another 14 h to give a yellowish-brown solution. The solution was filtered, and the solvent was evaporated under vacuum. The residue was washed with deionized water and Et_2O several times and dried under vacuum. The CH_2Cl_2 extract was recrystallized from $Et_2O/MeOH/CH_2Cl_2$ to give a sample of $[Et_4N]_2$[**6**] (yield 0.18 g, 0.12 mmol, 60% based on Pb).

Synthesis of $[Et_4N]_2[Ru_3(CO)_9\{PbCr(CO)_5\}_2]$ ($[Et_4N]_2$[7]). A MeOH solution (20 mL) of $Cr(CO)_6$ (0.15 g, 0.68 mmol) and KOH (5.31 g, 94.6 mmol) was stirred in an ice/water bath and warmed to ambient temperature. After 3 h, $PbCl_2$ (0.20 g, 0.72 mmol) was added to the solution, which was stirred for another 4 h to give a reddish-brown solution. $Ru_3(CO)_{12}$ (0.22 g, 0.34 mmol) was then added to the solution and stirred for 36 h at ambient temperature to yield a brown solution, which was filtered and concentrated, and an aqueous solution of $[Et_4N]Br$ (0.31 g, 1.48 mmol) was added dropwise, precipitating the solid. The solid was washed with deionized water several times and dried under vacuum. The CH_2Cl_2 extract was recrystallized from $Et_2O/MeOH/CH_2Cl_2$ to give a reddish-brown sample of $[Et_4N]_2$[**7**] (yield 0.20 g, 0.12 mmol, 35% based on Ru). IR (ν_{CO}, CH_2Cl_2): 2033 (m), 1970 (vs), 1923 (m), 1887 (m) cm^{-1}. Anal. Calcd for $[Et_4N]_2$[**7**]: C, 26.04; H, 2.50; N, 1.74. Found: C, 26.01; H, 2.71; N, 1.60. Crystals of $[Et_4N]_2$[**7**] suitable for X-ray diffraction were grown from Et_2O/CH_2Cl_2.

X-ray Structural Characterization of $[Bu_4N]_2$[3], $[Et_4N]_2$[4], $[Et_4N]_2$[5], $[Et_4N]_2$[6], and $[Et_4N]_2$[7]. Some selected crystallographic data for $[Bu_4N]_2$[**3**], $[Et_4N]_2$[**4**], $[Et_4N]_2$[**5**], $[Et_4N]_2$[**6**], and $[Et_4N]_2$[**7**] are given in Table 5. All crystals were mounted on glass fibers with epoxy cement. Data collection for $[Bu_4N]_2$[**3**] was carried out using a Nonius (CAD-4) diffractometer with graphite-monochromated Mo Kα radiation at 298 K in the 2θ range of 2.0−50° employing $\theta-2\theta$ scans, and an empirical absorption correction by azimuthal (Ψ) scans was applied.[29] Data collection for $[Et_4N]_2$[**4**], $[Et_4N]_2$[**5**], $[Et_4N]_2$[**6**], and $[Et_4N]_2$[**7**] was carried out using a Bruker-Nonius Kappa CCD diffractometer with graphite-monochromated Mo Kα radiation at 298 K, and an empirical absorption correction by multiscans was applied. The structures of $[Bu_4N]_2$[**3**], $[Et_4N]_2$[**4**], $[Et_4N]_2$[**5**], $[Et_4N]_2$[**6**], and $[Et_4N]_2$[**7**] were refined by *SHELXL* packages.[30] All of the non-H atoms of $[Bu_4N]_2$[**3**], $[Et_4N]_2$[**4**], $[Et_4N]_2$[**5**], $[Et_4N]_2$[**6**], and $[Et_4N]_2$[**7**] were refined with anisotropic temperature factors. Additional crystallographic data in the form of CIF files are available as Supporting Information.

Computational Details. All calculations reported in this study were performed via DFT with Becke's three-parameter (B3) exchange functional and the Lee−Yang−Parr (LYP) correlation functional (B3LYP)[21,22] using the *Gaussian 03* series of packages.[31] The geometries of complexes **1**−**7**, $[Cr(CO)_5]^{2-}$, $[Fe(CO)_4]^{2-}$, and $Ru_3(CO)_{12}$ and the proposed intermediates $[BrPb\{Cr(CO)_5\}_2]^-$ and $[Pb\{Cr(CO)_5\}\{Ru(CO)_4\}_2]^{2-}$ were fully optimized with the Stuttgart/Dresden relativistic effective core potential[32] and with the LanL2DZ basis set for Pb, Br, Cr, Fe, and Ru atoms and the 6-31G(d) basis set for C and O atoms. The optimized geometries were further confirmed by harmonic vibrational frequency analysis, obtained via analytical energy second derivatives. Wiberg bond indices[33] and natural charges[24] were evaluated using the Weinhold NBO method.[23] Graphical representations of the molecular orbitals were obtained using CS Chem3D 5.0.

Acknowledgment. This work was supported by the National Science Council of Taiwan (Grant 98-2113-M-003-006-MY3 to M.S.). We are also grateful to the National Center for High-Performance Computing, where the Gaussian package and computer time were provided.

Supporting Information Available: X-ray crystallographic files in CIF format for $[Bu_4N]_2$[**3**], $[Et_4N]_2$[**4**], $[Et_4N]_2$[**5**], $[Et_4N]_2$[**6**], and $[Et_4N]_2$[**7**], CV, equatorial plane of the structure of **5**, spatial graphs, and computational details for **1**−**7**, $[Cr(CO)_5]^{2-}$, $[Fe(CO)_4]^{2-}$, and $Ru_3(CO)_{12}$ and the proposed intermediates $[BrPb\{Cr(CO)_5\}_2]^-$ and $[Pb\{Cr(CO)_5\}\{Ru(CO)_4\}_2]^{2-}$. This material is available free of charge via the Internet at http://pubs.acs.org.

(29) North, A. C. T.; Philips, D. C.; Mathews, F. S. *Acta Crystallogr.* **1968**, *A24*, 351–359.

(30) Sheldrick, G. M. *SHELXL97*, version 97-2; University of Göttingen: Göttingen, Germany, 1997.

(31) Frisch, M. J.; Trucks, G. W.; Schlegel, H. B.; Scuseria, G. E.; Robb, M. A.; Cheeseman, J. R.; Montgomery, J. A., Jr.; Vreven, T.; Kudin, K. N.; Burant, J. C.; Millam, J. M.; Iyengar, S. S.; Tomasi, J.; Barone, V.; Mennucci, B.; Cossi, M.; Scalmani, G.; Rega, N.; Petersson, G. A.; Nakatsuji, H.; Hada, M.; Ehara, M.; Toyota, K.; Fukuda, R.; Hasegawa, J.; Ishida, M.; Nakajima, T.; Honda, Y.; Kitao, O.; Nakai, H.; Klene, M.; Li, X.; Knox, J. E.; Hratchian, H. P.; Cross, J. B.; Bakken, V.; Adamo, C.; Jaramillo, J.; Gomperts, R.; Stratmann, R. E.; Yazyev, O.; Austin, A. J.; Cammi, R.; Pomelli, C.; Ochterski, J. W.; Ayala, P. Y.; Morokuma, K.; Voth, G. A.; Salvador, P.; Dannenberg, J. J.; Zakrzewski, V. G.; Dapprich, S.; Daniels, A. D.; Strain, M. C.; Farkas, O.; Malick, D. K.; Rabuck, A. D.; Raghavachari, K.; Foresman, J. B.; Ortiz, J. V.; Cui, Q.; Baboul, A. G.; Clifford, S.; Cioslowski, J.; Stefanov, B. B.; Liu, G.; Liashenko, A.; Piskorz, P.; Komaromi, I.; Martin, R. L.; Fox, D. J.; Keith, T.; Al-Laham, M. A.; Peng, C. Y.; Nanayakkara, A.; Challacombe, M.; Gill, P. M. W.; Johnson, B.; Chen, W.; Wong, M. W.; Gonzalez, C.; Pople, J. A. *Gaussian 03*, revision B.04; Gaussian, Inc.: Wallingford, CT, 2004.

(32) (a) Schwerdtfeger, P.; Dolg, M.; Schwarz, W. H.; Bowmaker, G. A.; Boyd, P. D. W. *J. Chem. Phys.* **1989**, *91*, 1762–1774. (b) Andrae, D.; Häussermann, U.; Dolg, M.; Stoll, H.; Preuss, H. *Theor. Chim. Acta* **1990**, *77*, 123–141. (c) Bergner, A.; Dolg, M.; Kuechle, W.; Stoll, H.; Preuss, H. *Mol. Phys.* **1993**, *80*, 1431–1441.

(33) Wiberg, K. B. *Tetrahedron* **1968**, *24*, 1083–1096.